Available online at www.sciencedirect.com
ScienceDirect
Theoretical Population Biology 72 (2007) 214–230
Theoretical Population Biology
www.elsevier.com/locate/tpb

Dynamics and spatial organization of plant communities in water-limited systems

E. Gilad[a,b], M. Shachak[c], E. Meron[b,a,*]

[a]Department of Physics, Ben-Gurion University, Beer Sheva 84105, Israel
[b]Department of Solar Energy and Environmental Physics, BIDR, Ben Gurion University, Sede Boqer Campus 84990, Israel
[c]Mitrani Department of Desert Ecology, BIDR, Ben Gurion University, Sede Boqer Campus 84990, Israel

Received 16 August 2006
Available online 21 May 2007

Abstract

A mathematical model for plant communities in water-limited systems is introduced and applied to a mixed woody–herbaceous community. Two feedbacks between biomass and water are found to be of crucial importance for understanding woody–herbaceous interactions: water uptake by plants' roots and increased water infiltration at vegetation patches. The former acts to increase interspecific competition while the latter favors facilitation. The net interspecific interaction is determined by the relative strength of the two feedbacks. The model is used to highlight new mechanisms of plant-interaction change by studying factors that tilt the balance between the two feedbacks. Factors addressed in this study include environmental stresses and patch dynamics of the woody species. The model is further used to study mechanisms of species-diversity change by taking into consideration tradeoffs in species traits and conditions giving rise to irregular patch patterns.

Keywords: Mathematical modeling; Plant communities; Water-limited systems; Biomass–water feedbacks; Plant interactions; Aridity gradient; Competition vs. facilitation; Vegetation patterns; Species-diversity change

1. Introduction

The dynamics and spatial organization of plant communities strongly depend on intraspecific and interspecific interactions. Intraspecific interactions can lead to spatial self-organization resulting in vegetation patterns of various forms (Lefever and Lejeune, 1997; Klausmeier, 1999; Okayasu and Aizawa, 2001; von Hardenberg et al., 2001; Rietkerk et al., 2002; Gilad et al., 2004). A striking example is vegetation bands on hill slopes in arid and semi-arid regions (Valentin et al., 1999). Interspecific interactions can induce species competition or facilitation resulting in local exclusion or coexistence of species. Field studies of plant interactions along environmental gradients reveal a change from competition to facilitation (or from "negative" to "positive" plant interactions) as abiotic stresses or consumer pressures increase (Bertness and Callaway, 1994; Bertness and Hacker, 1994; Greenlee and Callaway, 1996; Callaway and Walker, 1997; Brooker and Callaghan, 1998; Pugnaire and Luque, 2001; Callaway et al., 2002; Bertness and Ewanchuk, 2002; Maestre et al., 2003). In water-limited systems such changes have been observed in woody–herbaceous communities under conditions of increased aridity. Facilitation in this case is manifested by the growth of annuals, grasses and other species under the canopy of woody plants (Pugnaire and Luque, 2001). Some other studies (Casper, 1996; Tielbörger and Kadmon, 2000; Pennings et al., 2003; Maestre and Cortina, 2004a, b) appear to be in conflict with this reported shift in plant interactions (Maestre et al., 2005).

Significant progress has been made in understanding vegetation patterns by means of mathematical modeling. Among the proposed models (Lefever and Lejeune, 1997;

*Corresponding author. Department of Solar Energy and Environmental Physics, BIDR, Ben Gurion University, Sede Boqer Campus 84990, Israel. Fax: +972 8 6596921.
E-mail addresses: gilade@bgu.ac.il (E. Gilad), shachak@bgu.ac.il (M. Shachak), ehud@bgu.ac.il (E. Meron).
URLs: http://physics.bgu.ac.il/~gilade (E. Gilad), http://www.bgu.ac.il/~ehud (E. Meron).

0040-5809/$ - see front matter © 2007 Elsevier Inc. All rights reserved.
doi:10.1016/j.tpb.2007.05.002

Klausmeier, 1999; von Hardenberg et al., 2001; Okayasu and Aizawa, 2001; Rietkerk et al., 2002; Shnerb et al., 2003; Gilad et al., 2004, 2007), most instrumental have been those that include water–biomass feedbacks (Okayasu and Aizawa, 2001; Rietkerk et al., 2002; Gilad et al., 2004). Two feedbacks have been found particularly significant; increased infiltration at vegetation patches (''infiltration feedback'') and water uptake by plants' roots (''uptake feedback''). Any of these feedbacks alone can induce spatial instabilities leading to biomass patterns; the uptake feedback does that by capturing root augmentation in response to biomass growth (Gilad et al., 2004, 2007). However, including both feedbacks and changing their relative strength can provide additional information about the capacity of plants in water-limited systems to act as ecosystem engineers (Gilad et al., 2004, 2007).

Despite the progress that has been made in understanding vegetation patterns (Rietkerk et al., 2004) and plant interactions along environmental gradients (Brooker and Callaghan, 1998), the spatio-temporal response of plant communities to environmental stresses and the underlying mechanisms are still poorly understood (House et al., 2003). Mathematical modeling of vegetation pattern formation has so far been limited to a single species population (Lefever and Lejeune, 1997; Klausmeier, 1999; Okayasu and Aizawa, 2001; von Hardenberg et al., 2001; Rietkerk et al., 2002; Gilad et al., 2004) whereas most models of interacting populations, beginning with the Lotka–Volterra model (Murray, 1993), have focused on competitive interactions (Tilman, 1982, 1988; Grover, 1997; Sommer and Worm, 2002), overlooking facilitation (Brooker and Callaghan, 1998; Bruno et al., 2003). In addition, cross-scale effects, such as the interplay between patch dynamics at the landscape level and species composition at the single-patch level, have hardly been addressed.

In this paper we introduce and study a nonlinear mathematical model for plant communities in water-limited systems. The model captures the infiltration and uptake water–biomass feedbacks and extends the single-population model reported by Gilad et al. (2004, 2007) to n-interacting populations. Using a two species version of the model we elucidate mechanisms of plant-interaction changes, induced by aridity stresses and disturbances, and highlight the interplay between intraspecific and interspecific interactions, and between landscape and single-patch dynamics. We further study the relations between species-interaction changes to species composition changes by modeling herbaceous-species traits, such as tolerances to shading and grazing.

2. A model for n-interacting plant populations

We consider a two-dimensional spatially extended system where the limiting resource is water, and assume the system contains n life forms of vegetation. Depending on the particular context, a life form can represent a single species or a functional group. We assume that the life forms are affected by environmental factors such as rainfall, topography, soil type, grazing, and clear-cutting, but do not feed back significantly on the atmosphere or on the topography and soil type (e.g. through erosion).

2.1. Description of the model

The model contains $n+2$ dynamical variables: n biomass variables, $B_i(\mathbf{X},T)$ $(i=1,\ldots,n)$, representing biomass densities above ground level of the n life forms in units of [kg/m^2], a soil-water variable, $W(\mathbf{X},T)$, describing the amount of soil water available to the plants per unit area of ground surface in units of [kg/m^2], and a surface water variable, $H(\mathbf{X},T)$, describing the height of a thin water layer above ground level in units of [mm]. The model equations are

$$\begin{aligned}
\frac{\partial B_i}{\partial T} &= G_B^i[B_i,W]B_i(1-B_i/K_i) - M_iB_i \\
&\quad + D_{B_i}\nabla^2 B_i, \quad i=1,\ldots,n, \\
\frac{\partial W}{\partial T} &= I(\{B_i\})H - L(\{B_i\})W - W\sum_{i=1}^{n} G_W^i[B_i] + D_W\nabla^2 W, \\
\frac{\partial H}{\partial T} &= P - I(\{B_i\})H + D_H\nabla^2(H^2) + 2D_H\nabla H\cdot\nabla Z \\
&\quad + 2D_H H\nabla^2 Z,
\end{aligned} \tag{1}$$

where $\{B_i\}$ stands for all biomass densities and $\nabla^2=\partial_X^2+\partial_Y^2$. The quantity G_B^i [yr^{-1}] represents the growth rate of the ith life form, G_W^i [yr^{-1}] represents its soil-water consumption rate, and K_i [kg/m^2] is its maximum standing biomass. The rates G_B^i and G_W^i are functionals of biomass and soil water as indicated (see Eqs. (3) and (4)). The quantity I [yr^{-1}] represents the infiltration rate of surface water into the soil, while L [yr^{-1}] represents the evaporation rate of soil water. Both I and L are functions of all biomass densities (see Eqs. (2) and (5)). The parameter P [mm/yr] stands for the precipitation rate, and assumes in this study constant values representing mean annual rainfall rates. The parameter M_i [yr^{-1}] describes the biomass-loss rate of the ith life form due to mortality and various disturbances (e.g. grazing). The terms $D_{B_i}\nabla^2 B_i$ and $D_W\nabla^2 W$ represent, respectively, local seed dispersal of the ith life form, and soil-water transport in non-saturated soil (Hillel, 1998). Finally, the non-flat ground surface height [mm] is described by the topography function $Z(\mathbf{X})$ where the parameter D_H [m^2/yr (kg/m^2)$^{-1}$] represents the phenomenological bottom friction coefficient between the surface water and the ground surface.

The equation for H was motivated by shallow water theory. The shallow water approximation is based on the assumption of a thin layer of water where pressure variations are very small and the motion becomes almost two-dimensional. In deriving the equation for H a linear dependence of the bottom friction on the velocity of surface water has been assumed (Gilad et al., 2004).

2.2. Modeling biomass–water feedbacks

Three biomass–water feedbacks are modeled in Eqs. (1) as described below:

(1) *infiltration feedback*: increased infiltration at vegetation patches,
(2) *uptake feedback*: water uptake by plants' roots, and
(3) *shading feedback*: reduced evaporation at vegetation patches.

The infiltration feedback is modeled through the explicit form of the infiltration rate I. A monotonously increasing dependence of I on biomass density is assumed in order to capture the positive nature of this feedback; the larger the biomass density the higher the infiltration rate and the more soil water available to the plants. Various factors contribute to the higher infiltration rate of surface water into vegetated soil as compared with bare soil, including biological crusts that grow on bare soil and reduce the infiltration rate (Campbell et al., 1989; West, 1990), and soil mounds, formed by litter accumulation and dust deposition, that intercept runoff (Yair and Shachak, 1987).

The explicit dependence of the infiltration rate on the biomass density is a generalization of the form used in Gilad et al. (2004):

$$I(\mathbf{X},T)=A\frac{\sum_i Y_i B_i(\mathbf{X},T)+Qf}{\sum_i Y_i B_i(\mathbf{X},T)+Q}, \tag{2}$$

where A [yr^{-1}], Q [$\mathrm{kg/m}^2$], Y_i, and f are constant parameters and $Y_1=1$. The dependence of the infiltration rate on the weighted biomass-density sum, $\sum_i Y_i B_i$, is shown in Fig. 1. Two distinct limits of this quantity are noteworthy. When $\sum_i Y_i B_i \to 0$, this quantity represents the infiltration rate in bare soil, $I=Af$. When $\sum_i Y_i B_i \gg Q$ it represents infiltration rate in fully vegetated soil, $I=A$.

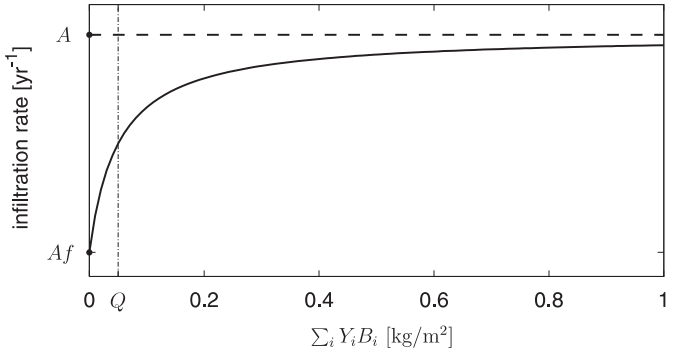

Fig. 1. The infiltration rate $I=A(\sum_i Y_i B_i+Qf)/(\sum_i Y_i B_i+Q)$ as a function of the weighted biomass-density sum $\sum_i Y_i B_i$. When the biomass is diminishingly small ($\sum_i Y_i B_i \ll Q$) the infiltration rate approaches the value of Af. When the biomass is large ($\sum_i Y_i B_i \gg Q$) the infiltration rate approaches A. The infiltration contrast between bare and vegetated soil is quantified by the parameter f, where $0<f<1$; when $f=1$ the contrast is zero (dashed line) and when $f=0$ the contrast is maximal. Small f values can model biological crusts which significantly reduce the infiltration rates in bare soils. Disturbances involving crust removal can be modeled by relatively high f values.

The parameter Q represents a reference biomass density beyond which the vegetation density approaches its full capacity to increase the infiltration rate. The infiltration contrast (between bare and vegetated soil) is quantified by the parameter f, defined to span the range $0<f<1$. When $f \ll 1$ the infiltration rate in bare soil is much smaller than the rate in vegetated soil. Such values can model bare soils covered by biological crusts (Campbell et al., 1989; West, 1990). As f gets closer to 1, the infiltration rate becomes independent of the biomass densities B_i. The parameter f measures the strength of the positive feedback due to increased infiltration at vegetation patches. The smaller f the stronger the feedback effect.

The uptake feedback is modeled through the explicit forms of the growth rate G_B^i and the consumption rate G_W^i. These forms capture the non-local nature of the uptake process by the root system, as well as the augmentation of the root system in response to biomass growth (Gilad et al., 2004, 2007). Water uptake obviously acts as a negative feedback; water availability increases biomass growth but biomass growth decreases water availability through water consumption. The uptake process, however, also act as a positive feedback when root augmentation is taken into account; as the biomass grows the root system extends in size, probes larger soil volumes, and take up more water. Besides providing a mechanism for vegetation pattern formation, independent of the infiltration-feedback mechanism, this aspect of water uptake is crucial for studying interspecific interaction changes in stressed environments.

The growth rate G_B^i at a point $\mathbf{X}$ at time T is modeled by the following non-local form:

$$G_B^i(\mathbf{X},T)=\Lambda_i\int_\Omega G_i(\mathbf{X},\mathbf{X}',T)W(\mathbf{X}',T)\,d\mathbf{X}',$$
$$G_i(\mathbf{X},\mathbf{X}',T)=\frac{1}{2\pi S_i^2}\exp\left[-\frac{|\mathbf{X}-\mathbf{X}'|^2}{2[S_i(1+E_iB_i(\mathbf{X},T))]^2}\right], \tag{3}$$

where Λ_i [$(\mathrm{kg/m}^2)^{-1}\,\mathrm{yr}^{-1}$] represents the plant's growth rate per unit amount of soil water, the Gaussian kernel $G_i(\mathbf{X},\mathbf{X}',T)$ represents the distribution of the root system, and the integration is over the entire physical domain Ω. According to this form, the biomass growth rate depends not only on the amount of soil water at the plant location, but also on the amount of soil water in the neighborhood spanned by the plant's roots. A measure for the root-system size [m] is given by $S_i(1+E_iB_i(\mathbf{X},T))$, where E_i [$(\mathrm{kg/m}^2)^{-1}$] quantifies the root augmentation per unit biomass, beyond a minimal root-system size S_i. The parameter E_i measures the strength of the positive uptake feedback due to root augmentation; the larger E_i the stronger the feedback effect of the ith species.

The soil-water consumption rate at a point $\mathbf{X}$ at time T is similarly given by

$$G_W^i(\mathbf{X},T)=\Gamma_i\int_\Omega G_i(\mathbf{X}',\mathbf{X},T)B_i(\mathbf{X}',T)\,d\mathbf{X}', \tag{4}$$

where Γ_i $[(\mathrm{kg/m^2})^{-1}\,\mathrm{yr}^{-1}]$ measures the soil-water consumption rate per unit biomass of the ith species. The soil-water consumption rate at a given point is due to all plants whose roots extend to this point. Note that $G_i(\mathbf{X}', \mathbf{X}, T) \neq G_i(\mathbf{X}, \mathbf{X}', T)$.

The shading feedback is captured by the following biomass dependence of the soil-water evaporation rate:

$$L(\mathbf{X}, T) = \frac{N}{(1 + \sum_{i=1}^{n} R_i B_i / K_i)}, \tag{5}$$

where N $[\mathrm{yr}^{-1}]$ is the evaporation rate in bare soil. The reduction in evaporation rate due to shading by the ith life form is quantified by the parameter R_i. Throughout this study we assume that the shading feedback is sufficiently weak for the following linear approximation to be valid:

$$L(\mathbf{X}, T) \approx N\left(1 - \sum_{i=1}^{n} R_i B_i / K_i\right). \tag{6}$$

The shading feedback is positive, but unlike the infiltration feedback, the increased soil-water density under a vegetation patch, due to reduced evaporation, does not involve depletion of soil water in the patch neighborhood. As a consequence, the shading feedback is not expected to induce spatial instabilities leading to vegetation patterns.

2.3. Non-dimensional form of the model

It is advantageous to express the model equations (1) in terms of non-dimensional variables and parameters as defined in Table 1. The non-dimensional form of the model equations is

$$\begin{aligned}
\frac{\partial b_i}{\partial t} &= G_b^i b_i(1 - b_i) - \mu_i b_i + \delta_{b_i} \nabla^2 b_i, \quad i = 1, \ldots, n,\\
\frac{\partial w}{\partial t} &= \mathcal{I} h - v\left(1 - \sum_{i=1}^{n} \rho_i b_i\right) w - w \sum_{i=1}^{n} G_w^i + \delta_w \nabla^2 w,\\
\frac{\partial h}{\partial t} &= p - \mathcal{I} h + \delta_h \nabla^2 (h^2) + 2\delta_h \nabla h \cdot \nabla \zeta + 2\delta_h h \nabla^2 \zeta,
\end{aligned} \tag{7}$$

where $\nabla^2 = \partial_x^2 + \partial_y^2$ and t and $\mathbf{x} = (x, y)$ are the non-dimensional time and spatial coordinates. The infiltration term now reads

$$\mathcal{I}(\mathbf{x}, t) = \alpha \frac{\sum_i \psi_i b_i(\mathbf{x}, t) + qf}{\sum_i \psi_i b_i(\mathbf{x}, t) + q}, \tag{8}$$

the growth-rate term G_b^i is

$$\begin{aligned}
G_b^i(\mathbf{x}, t) &= v\lambda_i \int_\Omega g_i(\mathbf{x}, \mathbf{x}', t) w(\mathbf{x}', t)\, d\mathbf{x}',\\
g_i(\mathbf{x}, \mathbf{x}', t) &= \frac{1}{2\pi\sigma_i^2} \exp\left[-\frac{|\mathbf{x} - \mathbf{x}'|^2}{2[\sigma_i(1 + \eta_i b_i(\mathbf{x}, t))]^2}\right],
\end{aligned} \tag{9}$$

and the soil-water consumption rate is

$$G_w^i(\mathbf{x}, t) = \gamma_i \int_\Omega g_i(\mathbf{x}', \mathbf{x}, t) b_i(\mathbf{x}', t)\, d\mathbf{x}'. \tag{10}$$

Table 1
Relations between non-dimensional variables and parameters and the dimensional ones appearing in the dimensional form of the model equations (1)–(4)

Quantity	Scaling
b_i	B_i/K_i
w	$\Lambda_1 W/N$
h	$\Lambda_1 H/N$
v	N/M_1
λ_i	Λ_i/Λ_1
μ_i	M_i/M_1
α	A/M_1
q	Q/K_1
$\mathbf{x}$	$\mathbf{X}/\mathbf{S_1}$
t	$M_1 T$
p	$\Lambda_1 P/NM_1$
γ_i	$\Gamma_i K_i/M_1$
η_i	$E_i K_i$
ρ_i	R_i
σ_i	S_i/S_1
δ_{b_i}	$D_{B_i}/M_1 S_1^2$
δ_w	$D_W/M_1 S_1^2$
δ_h	$D_H N/M_1 \Lambda_1 S_1^2$
ψ_i	$Y_i K_i/K_1$
ζ	$\Lambda_1 Z/N$

Note that according to these relations $\lambda_1 = \mu_1 = \sigma_1 = 1$.

3. Applying the model to woody–herbaceous ecosystems

Motivated by recent field studies of plant interactions in woody–herbaceous communities along aridity gradients (Pugnaire and Luque, 2001), we consider a system of two species ($n = 2$), representing woody vegetation (b_1) and herbaceous vegetation (b_2). Accordingly we choose the maximum standing biomass of the woody species to be an order of magnitude higher than that of the herbaceous species while its growth and mortality rates are taken to be significantly slower. We confine ourselves to the case of strong infiltration feedback ($f \ll 1$) and moderate uptake feedback of the woody species ($\eta_1 \sim \mathcal{O}(1)$). These conditions are often realized in drylands where biological soil crusts increase the infiltration contrast and the woody vegetation consists of shrubs (Shachak et al., 1998). With this parameter choice we find that the herbaceous vegetation is strongly affected by the woody vegetation, but the woody vegetation is hardly affected by the herbaceous one. The specific parameter values used in this paper, except otherwise mentioned, are: $v = \delta_w = 1.667$, $\alpha = 16.667$, $q = 0.05$, $f = 0.1$, $\delta_h = 416.667$, $\eta_1 = 3.5$, $\eta_2 = 0.35$, $\gamma_1 = 2.083$, $\gamma_2 = 0.208$, $\rho_1 = 0.95$, $\rho_2 = \psi_2 = 0.005$, $\delta_{b_1} = \delta_{b_2} = 0.167$, $\sigma_2 = 1$, $\lambda_2 = 10$ and $\mu_2 = 4.1$. These choices are motivated by earlier studies of woody–herbaceous systems in drylands (Sternberg and Shoshany, 2001; Hillel, 1998; Rietkerk et al., 2002). In all simulations we used periodic boundary conditions and domain sizes corresponding to $7.5 \times 7.5\,\mathrm{m}^2$. We note that the model solutions described here are robust and do not depend on delicate tuning of any particular parameter.

Eqs. (7) for $n=2$ have four stationary uniform solutions:

- $\mathcal{B}$: bare soil ($b_1=0, b_2=0$).
- $\mathcal{V}_1$: uniform woody vegetation ($b_1\neq 0, b_2=0$).
- $\mathcal{V}_2$: uniform herbaceous vegetation ($b_1=0, b_2\neq 0$).
- $\mathcal{M}$: uniform mixed woody–herbaceous vegetation ($b_1\neq 0, b_2\neq 0$).

These are displayed in the bifurcation diagram shown in Fig. 2 with p as the control parameter. The bare-soil solution, $\mathcal{B}$, is given by

$$b_1=0, \quad b_2=0, \quad w=p/v, \quad h=p/\alpha f. \tag{11}$$

The linear stability of this solution is determined by the dynamics of small non-uniform perturbations of the form $(\delta b_1, \delta b_2, \delta w, \delta h)^{\mathrm{T}} = \mathbf{a}\exp[\theta(k)t + \mathrm{i}\mathbf{k}\cdot\mathbf{x}] + \text{c.c.}$, where $\theta(k)$ is the growth rate of a perturbation characterized by a wavenumber $k=|\mathbf{k}|$, $\mathbf{a}$ is a constant vector, and "c.c." stands for the complex conjugate. We refer the reader to the Appendix for the calculation of the growth rates (eigenvalues) of perturbations along different modes. The outcomes of this calculation are

$$\theta_1(k) = p - 1 - \delta_{b_1}k^2, \tag{12}$$

determining the growth rate of woody vegetation, and

$$\theta_2(k) = \lambda_2 p - \mu_2 - \delta_{b_2}k^2, \tag{13}$$

determining the growth rate of herbaceous vegetation (two additional eigenvalues are always negative and do not affect the stability of the bare-soil solution).

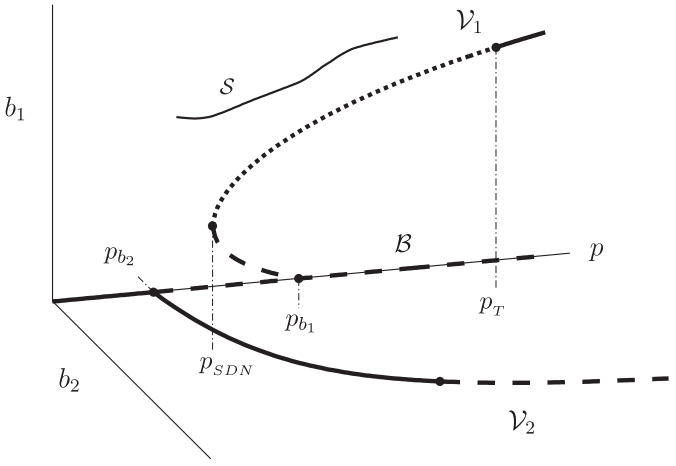

Fig. 2. Bifurcation diagram showing homogeneous and pattern solutions of the woody–herbaceous system. The solution branches $\mathcal{B}$, $\mathcal{V}_1$ and $\mathcal{V}_2$ represent, respectively, uniform bare soil, uniform woody vegetation and uniform herbaceous vegetation. The branch $\mathcal{S}$ represents the amplitudes of spots patterns. Solid lines represent stable solutions, and dashed and dotted lines represent solutions unstable to uniform and non-uniform perturbations, respectively. The thresholds $p_{b_2}=\mu_2/\lambda_2$ and $p_{b_1}=1$ correspond to 307.5 and 750 mm/yr, respectively. The points p_{SDN} and p_T denote, respectively, the saddle-node bifurcation and the finite-wavenumber instability along the uniform woody-vegetation branch $\mathcal{V}_1$.

Both θ_1 and θ_2 can become positive as p is increased from zero, implying instabilities of the bare-soil solution to vegetation growth. If $\mu_2/\lambda_2<1$ (the case considered in this work) the bare-soil solution first loses stability to the growth of uniform herbaceous vegetation. The threshold of this instability, $p=p_{b_2}$, is determined by the equation $\theta_2(0)=0$ whose solution gives $p_{b_2}=\mu_2/\lambda_2$. Fig. 3a shows the growth-rate curves, $\theta_2=\theta_2(k)$, below, at and above p_{b_2}. The curve at p_{b_2} shows that the first wavenumber to grow is $k=0$ indicating an instability to *uniform* herbaceous vegetation ($\mathcal{V}_2$). If $\mu_2/\lambda_2>1$, the bare-soil solution first loses stability to the growth of uniform woody vegetation ($\mathcal{V}_1$) and the instability threshold is $p=p_{b_1}=1$.

The calculation of the other solutions and their linear stability analyses are described in the Appendix. The bifurcation diagram in Fig. 2 shows the three solution branches, bare soil ($\mathcal{B}$), uniform woody vegetation ($\mathcal{V}_1$) and uniform herbaceous vegetation ($\mathcal{V}_2$), and their stability properties. Also shown is a non-uniform solution branch ($\mathcal{S}$) evaluated by numerically solving Eqs. (7). This solution branch describes a woody spot pattern at relatively low and high p values, and a mixed woody–herbaceous spot pattern at intermediate p values. Throughout this paper we confine ourselves to a parameter regime where stable spot patterns coexist with stable uniform herbaceous vegetation. Not shown in the diagram is the uniform mixed vegetation solution ($\mathcal{M}$) which is always unstable in the parameter regime considered in this work.

The form of the $\mathcal{V}_1$ branch indicates that the bifurcation of the bare-soil solution to uniform woody vegetation is subcritical. The criterion for subcriticality and the associated saddle-node bifurcation at $p=p_{SDN}$ are discussed in the Appendix. Subcritical bifurcations often imply bistability of states and hysteresis phenomena. In the present context, however, this is not the case (even when $\mu_2/\lambda_2>1$) because the part of the $\mathcal{V}_1$ branch that is stable to uniform perturbations (dotted part) is unstable to non-uniform

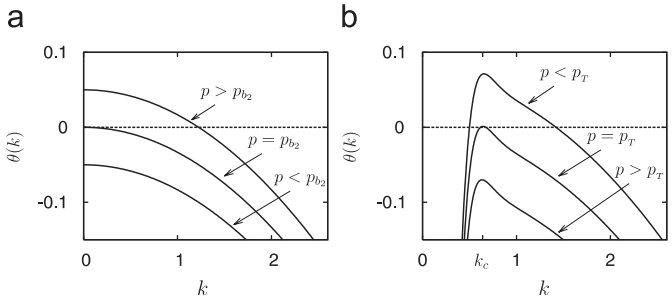

Fig. 3. Growth rates of non-uniform perturbations (a) about the bare-soil solution $\mathcal{B}$ near the bifurcation point $p=p_{b_2}$, and (b) about the uniform woody-vegetation solution $\mathcal{V}_1$ near the bifurcation point $p=p_T$ (see Fig 2). The growth rates, as functions of the perturbations' wavenumbers k, are given by the largest eigenvalues of the corresponding Jacobian matrices (Eq. (A.29)). As p is increased past $p=p_{b_2}$ a zero mode ($k=0$) begins to grow, implying an instability of the bare-soil solution to uniform perturbations (a). As p is decreased past $p=p_T$ a finite-wavenumber mode ($k=k_c$) begins to grow, implying an instability of the uniform woody-vegetation solution to non-uniform perturbations (b).

perturbations due to a Turing-like instability at $p = p_T$. Growth-rate curves demonstrating this instability are shown in Fig. 3b.

4. Plant interactions in stressed environments

We consider plant interactions at three different levels: single-patch, a few interacting patches, and landscape. At the single-patch level we study how interspecific interactions change along aridity gradients (Sections 4.1 and 4.2). At the level of a few interacting patches we study the impact of intraspecific woody competition on interspecific interactions (Section 4.3). Finally, at the landscape level we study how global pattern transitions feed back to the level of a single patch and affect interspecific interactions.

4.1. From competition to facilitation along aridity gradient

We first reproduce an interaction trend observed in field studies, whereby competitive interspecific plant-interactions change to facilitative as environmental stresses increase (Bertness and Callaway, 1994; Bertness and Hacker, 1994; Greenlee and Callaway, 1996; Callaway and Walker, 1997; Brooker and Callaghan, 1998; Pugnaire and Luque, 2001; Callaway et al., 2002; Bertness and Ewanchuk, 2002; Maestre et al., 2003). We associate plant competition (facilitation) with cases where the soil-water density under a patch of woody vegetation is lower (higher) than the density in the surrounding bare soil. Fig. 4a shows results of simulating the model at decreasing precipitation values starting the simulations with initial states including no herbaceous (b_2) vegetation. The line $\mathcal{B}$ shows the soil-water content in bare soil while the line $\mathcal{S}$ shows the maximal water density under a b_1 patch. The two lines intersect at $p = p_f$ suggesting a crossover from competition at high precipitation ($p > p_f$), where the soil-water density under a b_1 patch is lower than in bare soil, to facilitation at low precipitation ($p < p_f$), where the soil-water density under a patch exceeds that of bare soil.

Figs. 4b,c show examples of spatial profiles of b_1 and w in the competition range (c) and in the facilitation range (b). Note that the line $\mathcal{S}$ terminates at some low precipitation value. Below that value the woody vegetation (b_1) no longer survives the dry conditions and a catastrophic shift (Scheffer et al., 2001) to bare soil occurs.

The model offers the following explanation for this crossover. As the system becomes more arid, the b_1 patch area becomes smaller and the water uptake decreases significantly. The infiltration rate at the reduced patch area, however, decreases only slightly because of its weak biomass dependence for $b_1 \gg q$ (see Fig. 1). As a result a given area of a b_1 patch in a more arid environment traps nearly the same amount of surface water, but a significantly smaller amount of soil water is consumed in that unit area due to fewer b_1 individuals in the surrounding region, as demonstrated in Fig. 5. The outcome is an increased soil-water density at the b_1 patch area which the b_2 species can benefit from. Two factors prevent from the b_1 species to exhaust the soil water for its own growth; its maximum standing biomass (K_1 in the dimensional model) which limits the local growth, and the depletion of soil water in the immediate vicinity of the b_1 patch which prevents its expansion. We assume here that K_1 represents factors that limit the woody-species growth but do not limit the herbaceous-species growth. A possible example of such a factor is a developmental strategy of dryland woody species to limit resource exploitation and growth during wet seasons in order to survive the dry seasons that follow.

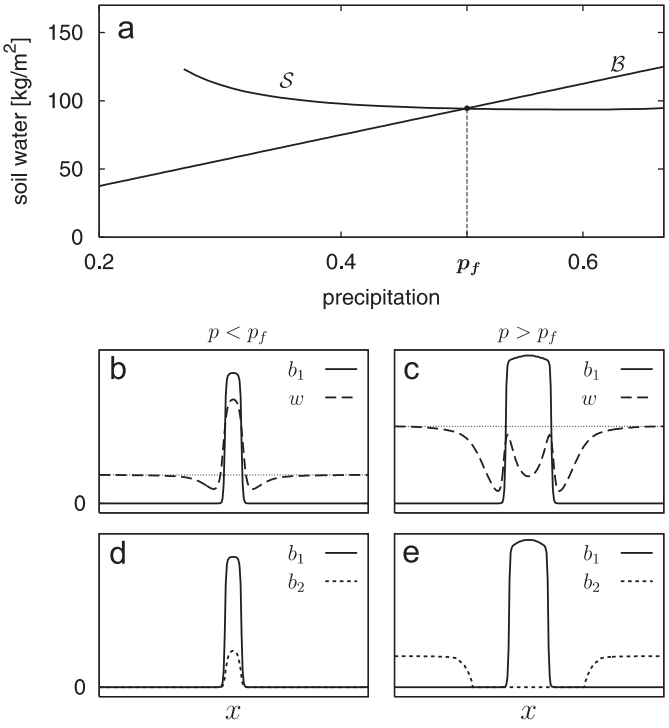

Fig. 4. Model solutions showing a transition from competition to facilitation as precipitation decreases. The lines $\mathcal{B}$ and $\mathcal{S}$ in panel (a) show, respectively, the soil-water density in bare soil and under a b_1 patch (in the absence of b_2) as functions of precipitation. Above (below) $p = p_f$ the water content under the b_1 patch is lower (higher) than in bare soil, implying competition (facilitation). Panels b–e show spatial profiles of b_1, b_2 and w in the competition range $p > p_f$ (c,e) where an herbaceous species b_2 is excluded by the woody species b_1, and in the facilitation range $p < p_f$ (b,d) where b_2 grows under the b_1 canopy. Precipitation values are: $p = 0.25$ (187.5 mm/yr) for b,d, $p = 0.6$ (450 mm/yr) for c,e, and $p_f = 0.5$ (378 mm/yr).

Simulations of the model equations with small randomly distributed initial b_2 biomass, indeed show a transition from competition at $p > p_f$, where the b_1 species excludes the b_2 species from its patches and their immediate neighborhoods (Fig. 4e), to facilitation at $p < p_f$, where the b_2 species cannot survive the aridity stress and can only grow in patches of the b_1 species (Fig. 4d). In this range the woody vegetation acts as an ecosystem engineer (Jones et al., 1994, 1997; Gurney and Lawton, 1996); it modifies the physical environment by redistributing the water resource, thereby creating habitats for herbaceous species.

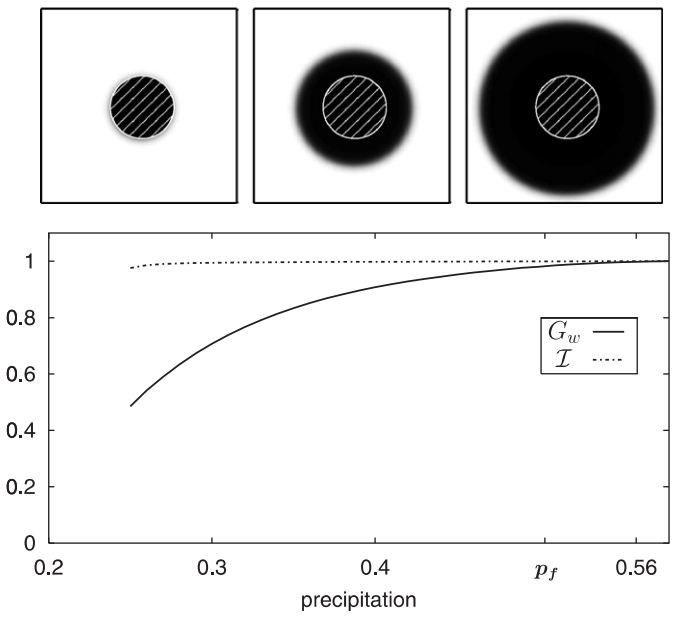

Fig. 5. Water balance under a woody patch along an aridity gradient, calculated using the model equations. Shown are the water uptake rate G_w (solid line) and the water infiltration rate $\mathcal{I}$ (dotted line) per constant area size (hatched circles in upper panels) in a b_1 patch as precipitation changes. As the system becomes more arid, the b_1 patch area becomes smaller (see upper panels) and the water uptake from the same area size decreases significantly. The infiltration rate, however, decreases only slightly. Consequently, the soil-water density per unit area of a woody patch increases as the system becomes more arid. The values of G_w and $\mathcal{I}$ are normalized with respect to their maximal value and correspond to the model solutions denoted by the $\mathcal{S}$ curve in Fig. 4. The asymptotic patches shown in the upper panels (from left to right) were calculated at precipitation values 0.25 (187.5 mm/yr), 0.45 (337.5 mm/yr) and 0.65 (487.5 mm/yr).

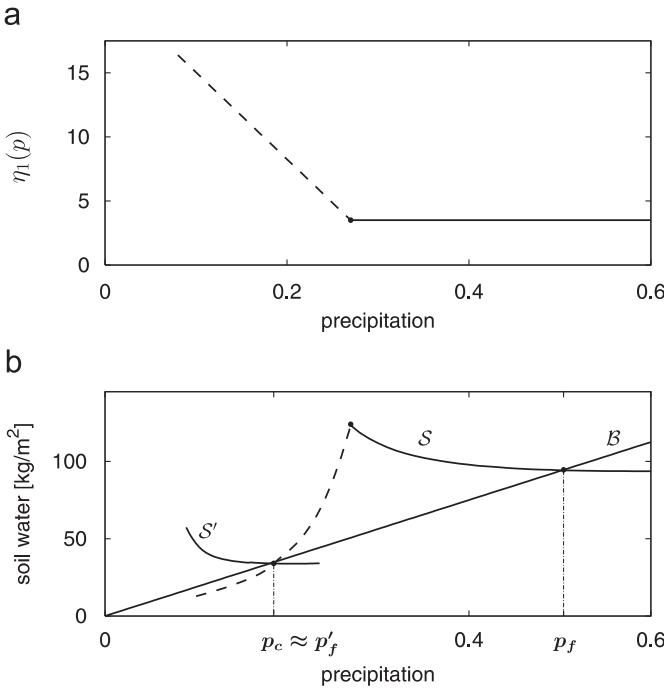

Fig. 6. Transition back to competition at extreme aridity, obtained by introducing a functional dependence of the root extension parameter η_1 on the precipitation rate p (panel a). The increase in η_1 at low p (dashed line) improves the resilience of b_1 plants to aridity stresses, but decreases the soil-water content under their patches (dashed part of the $\mathcal{S}$ line in panel b). Transition back to competition occurs below the second crossing point of the $\mathcal{B}$ and $\mathcal{S}$ lines, $p_c < p_f$ (p_c corresponds to 140 mm/yr). The $\mathcal{S}'$ line shows the soil-water content under the patches of another b_1 species for which the upper crossing point, p'_f (competition to facilitation), is close to the lower crossing point, p_c (facilitation to competition), of the first species. Under such circumstances both directions of plant-interaction change, competition to facilitation and facilitation to competition, can be realized along the same rainfall gradient.

4.2. Back to competition

The transition from competition to facilitation as precipitation decreases (Fig. 4) was obtained assuming that the parameter η_1, measuring the capacity of the woody vegetation to extend its roots as it grows, is independent of the precipitation p. Most dryland plants, however, have developed the capability to further extend their root systems in response to aridity stresses (Bloom et al., 1985). Fig. 6a shows a schematic dependence of η_1 on p that accounts for such a capability. The increased value of η_1 at low p improves the resilience of b_1 plants to aridity stresses as they are now capable of uptaking more soil water from their surroundings. The improved resilience is accompanied, however, by a decrease in the soil-water density under a b_1 patch (dashed part of the line $\mathcal{S}$ in Fig. 6b), and when the increase in η_1 at low p is steep enough, another crossing point, p_c, of the $\mathcal{B}$ and $\mathcal{S}$ lines may appear. Thus, depending on the particular $\eta_1(p)$ dependence, some woody species may show a transition back to competition as the aridity stress further increases.

The specific form of the $\mathcal{S}$ line may depend on other species traits as well. A species with a higher growth rate, for example, is characterized by an $\mathcal{S}'$ line that is shifted to lower precipitation values. Such a species may have a crossing point p'_f (competition to facilitation) close to the crossing point p_c (facilitation to competition) of another species, as shown in Fig. 6b. In such cases both directions of plant-interaction change, competition to facilitation and facilitation to competition, can be realized along the same environmental gradient, as field observations suggest (Maestre et al., 2005).

4.3. Interspecific facilitation induced by intraspecific competition

So far we considered interspecific interactions at the level of a single patch. At the level of a few interacting patches, competition over the soil-water resource among the woody patches can exert water stress on each patch. The effect of this "biotic" water stress is similar to the effect discussed in the previous subsections of an abiotic aridity stress on a single, isolated patch. Fig. 7 shows the response of an herbaceous species b_2 to sparse (a) and dense (b) woody patches b_1. When the patches are sufficiently sparse and effectively isolated, the b_1 species competes with the b_2 species and excludes it (Fig. 7a). However, when the

patches are dense enough, coexistence of the two species within the patches becomes possible (Fig. 7b). The competition for water reduces the b_1 patch size and consequently the soil-water consumption (see Fig. 5). As a result, more soil water is left for the b_2 species allowing its coexistence with the b_1 species.

The facilitation of the herbaceous species in the case of dense woody patches can be a *transient* phenomenon (Callaway and Walker, 1997) if the initial dense group of woody patches is isolated, as shown in Fig. 8. The woody patches at the group boundary tend to grow toward the surrounding open space. As the b_1 patches grow in size they consume more water and exclude the b_2 species. Along with this process the distances between nearby patches increase; the newly added woody individuals increase the competition over the water resource and lead to the dieback of woody individuals at any patch side that faces other patches. Thus species coexistence within the patches gradually turns into species exclusion, or facilitation turns into competition. This transient dynamics can be very slow, hundreds of years in the model simulations.

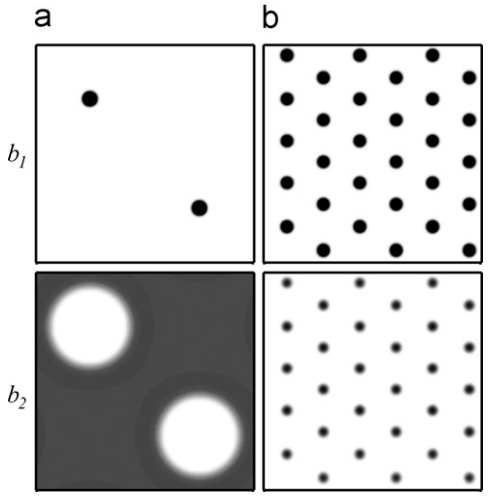

Fig. 7. Model solutions showing a transition from competition to facilitation as a result of a biotic stress. Shown are the spatial distributions of the two biomass densities, b_1 and b_2, for sparsely scattered b_1 patches (a) and for a closely packed hexagonal pattern of b_1 patches (b). The biotic stress results from intraspecific competition among b_1 patches over the water resource. The smaller b_1 patch size in case (b) reflects a stronger stress. For the chosen environment and species traits, the b_2 species is excluded from b_1 patches and their close neighborhoods when the patches are sparsely scattered, but coexists with b_1 (within its patches) when the patches are closely packed. The biotic stress, associated with intraspecific b_1-patch competition, leads to interspecific facilitation. The parameters used are given in the text except for: $v = \delta_w = 3.333$, $\alpha = 33.333$, $\delta_h = 333.333$, $\gamma_1 = 8.333$, $\gamma_2 = 0.833$, $\delta_{b_1} = \delta_{b_2} = 0.033$, $\mu_2 = 4.3$ and $p = 0.55$ (82.5 mm/yr).

4.4. Spatial patterning effects

At the landscape level, symmetry breaking vegetation patterns can appear (Gilad et al., 2004; Rietkerk et al., 2004). At this scale environmental stresses or consumer pressures may affect interspecific interactions by shifting the system from one pattern state to another. Fig. 9 (top row) shows a global transition from vegetation bands to vegetation spots of the woody species on a slope as a result of a local clear-cut along one of the bands. The mechanism of this transition is as follows (Gilad et al., 2004, 2007). The clear-cut allows for more runoff to accumulate at the band segment just below it. As a result this segment grows faster, draws more water from its surrounding and induces vegetation decay at the nearby band segments. The decay of the vegetation in the nearby segments allow for more runoff to accumulate at the next band downhill. The whole process continues repeatedly until the whole pattern transforms into a spot pattern. As shown in Gilad et al. (2007), the transition to spots is accompanied by higher soil-water densities under vegetation patches for each spot experiences a bare area uphill twice as large as the bare area between successive bands, and therefore absorbs more runoff.

Simulations of the model equations (7) indeed show that herbaceous species (b_2) that are excluded by the woody species (b_1) in the banded pattern can coexist with the woody species in the spotted pattern (Fig. 9, bottom row).

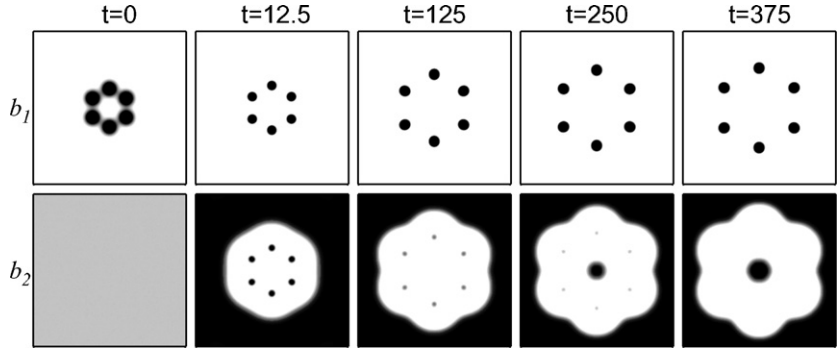

Fig. 8. Interspecific facilitation induced by intraspecific competition as a *transient* phenomenon. Shown are snapshots of the evolution in time of an isolated group of b_1 patches. Due to intraspecific competition among b_1 patches within the group they tend to grow toward the surrounding open space, thus increasing the distances between them and reducing the stress they exert on one another by water uptake. As a consequence, the b_1 patches grow in size, consume more water and exclude the b_2 species. Parameters used are as in Fig. 7 and t is in years.

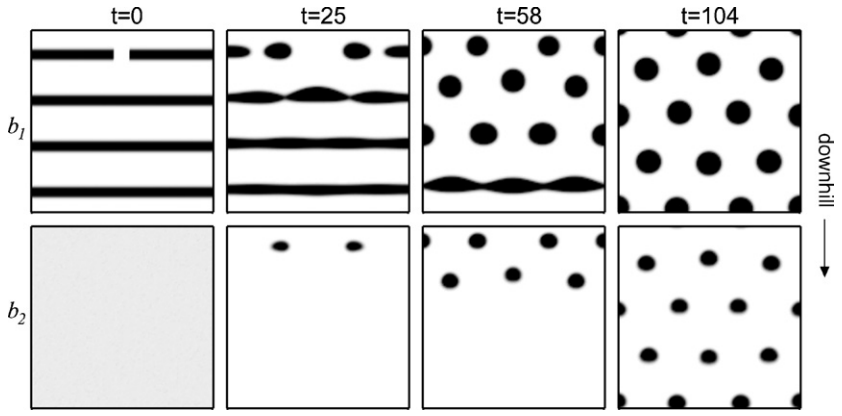

Fig. 9. Facilitation induced by a pattern shift at the landscape level. Shown is a sequence of snapshots at different times (t is in years) describing a transition from vegetation bands to vegetation spots on a slope induced by a local clear-cut along one of the bands (b_2 is randomly distributed at $t = 0$). In the banded pattern the b_1 species excludes the b_2 species, but in the spotted pattern they coexist due to enhanced runoff concentration. The slope angle is 15°, the precipitation is $p = 1.6$ (240 mm/yr) and all other parameters are as in Fig. 7 except for $\gamma_1 = 16.667$, $\gamma_2 = 1.667$, and $\mu_2 = 4.8$.

The transition from banded to spotted vegetation involves, in effect, a *facilitation front* propagating downhill; as bands gradually break into spots patches with higher soil-water density are formed, facilitating the growth of herbaceous species. This is an example of a cross-scale effect where pattern transitions at the landscape scale change interspecific interactions at the single-patch scale. The fact that the transition from bands to spots takes place at *constant* environmental conditions (including precipitation), indicates it is a pure spatial patterning effect rather than a single-patch facilitation induced by an aridity stress as discussed earlier.

5. Mechanisms of species-diversity change in stressed environments

Transitions from competition to facilitation as described in Section 4.1 are likely to involve changes in species composition. The results shown in Figs. 4d,e apply to herbaceous species whose growth is solely limited by water availability. Consider two additional factors that can limit the growth of herbaceous species; grazing and shading. A species sensitive to grazing can be modeled by assigning it a relatively high biomass-loss rate except in woody patches, where it is protected by the woody canopies. For simplicity we choose a linear relationship, $\mu_2 = \mu_{20} - \mu_{21} b_1$. Similarly, a species sensitive to shading (i.e. in need for abundant sunlight) can be modeled by assigning it a relatively high growth rate except in woody patches, $\lambda_2 = \lambda_{20} - \lambda_{21} b_1$.

We repeated the model simulation shown in Figs. 4d,e, once with a shading-sensitive herbaceous species whose biomass density is denoted by b_{2S}, and once with a grazing-sensitive species whose biomass density is denoted by b_{2G}. We use the following parameter values: $\mu_{20} = 5.5$, $\mu_{21} = 2.25$ and $\lambda_{20} = \lambda_{21} = 10$. The results are shown in Fig. 10. The b_2 species, whose growth is solely limited by water, is excluded by the woody species b_1 for $p > p_f$ but grows under its canopy for $p < p_f$ (Figs. 10a,b). The b_{2S} species, that grow in the competition range ($p > p_f$) away from the woody patches, cannot survive the shading under the woody canopies in the facilitation range ($p < p_f$), and disappears as a result of the transition from competition to facilitation (Figs. 10c,d). By contrast, the b_{2G} species, that cannot survive the open areas in the competition range, appears and grows under the canopies of the woody patches in the facilitation range (Figs. 10e,f).

Interspecific facilitation of herbaceous species may also result from intraspecific competition between woody patches at fixed environmental conditions (see Section 4.3). When the patches are far from one another, the woody species competes with the herbaceous species and excludes them. In this case, the b_{2G} species goes extinct, for it cannot survive the grazing stress in the open areas where it is not excluded by the woody species. The b_{2S} species, on the other hand, can grow in the unshaded open areas where the soil-water density is high, as Fig. 11a demonstrates (b_{2S} marked in yellow). When the patches are close enough, the intraspecific competition of the woody species for water reduces the sizes of its patches and consequently the soil-water consumption, giving rise to facilitation of herbaceous species in these patches. In this case, however, only the b_{2G} species can survive as Fig. 11b shows (b_{2G} marked in purple). The b_{2S} species goes extinct for it cannot survive the shading under the mesic woody canopies nor the dry unshaded open areas. Herbaceous species insensitive to grazing and shading (b_2) are likely to appear both in sparse and dense b_1 patch patterns (see Fig. 7).

Irregular patterns, involving regions of sparse and dense patches, can accommodate both types of species (b_{2S} and b_{2G}) as Fig. 11c shows, thus increasing the diversity of herbaceous species. This finding is consistent with the niche approach to biodiversity theory (Silvertown, 2004) where diversity is often linked to system heterogeneity. Irregular patch patterns exist in bistability ranges of uniform herbaceous vegetation and mixed spot patterns, and can

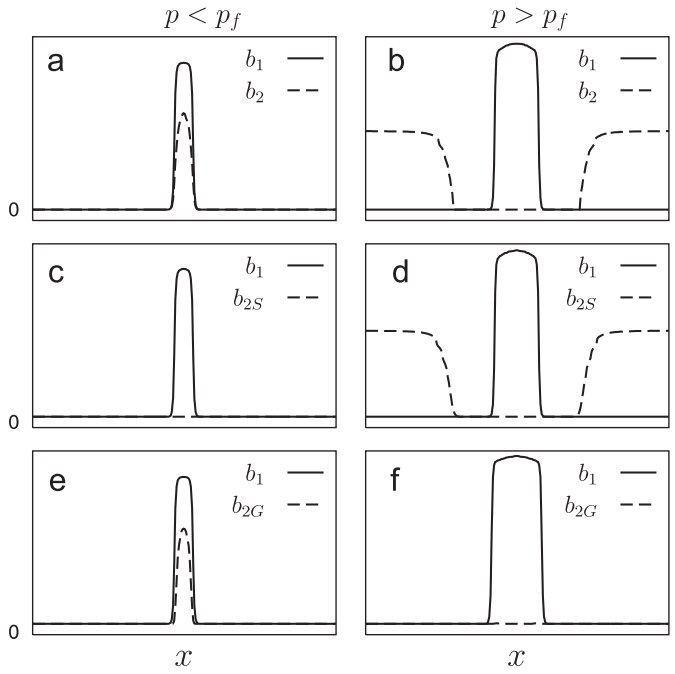

Fig. 10. Herbaceous-species composition changes induced by a precipitation drop from the competition range, $p>p_f$, to the facilitation range, $p<p_f$. Panels a,c,e (b,d,f) show spatial profiles of the woody (b_1) and the herbaceous (b_2) species below (above) p_f. An herbaceous species whose growth is solely limited by water, is excluded by the woody species for $p>p_f$ but grows under its canopy for $p<p_f$ (a,b). An herbaceous species b_{2S}, whose growth is also limited by shading, survives away from a woody patch for $p>p_f$, but disappears for $p<p_f$ (c,d). A species b_{2G}, whose growth is limited by grazing, cannot survive the woody competition and the grazing stress for $p>p_f$, but can grow under woody canopies for $p<p_f$ (f,g). Precipitation values are: $p = 0.25$ (187.5 mm/yr) for a,c,e, $p = 0.6$ (450 mm/yr) for b,d,f, and $p_f = 0.5$ (378 mm/yr).

be maintained in the field by appropriate clear-cutting and grazing management.

Variations in herbaceous-species composition can also result from transients involving changes in woody-patch density. The woody-patch "repulsion" shown in Fig. 8 implies, for example, the disappearance of a grazing-sensitive species (b_{2G}) on a time scale of hundreds of years.

6. Discussion

We presented here a mathematical model for the dynamics of a plant community involving n-interacting populations in water-limited systems. Two ingredients of the model are particularly significant for understanding plant interactions and their implications for species diversity: the infiltration feedback and the uptake feedback. Each feedback, independently of the other, induces intraspecific interactions that lead to similar spatial patterns at the landscape level. The two feedbacks differ, however, in the interspecific interactions they induce. The infiltration feedback induces positive interactions (facilitation) by trapping surface water in vegetation patches, thereby increasing the soil-water resource in these patches, and creating habitats for other vegetation species. The uptake feedback induces negative interactions (competition) by exploiting the soil-water resource and depleting its content in and around vegetation patches. Thus, dominance of the uptake feedback leads to competition and exclusion, whereas dominance of the infiltration feedback results in facilitation and coexistence.

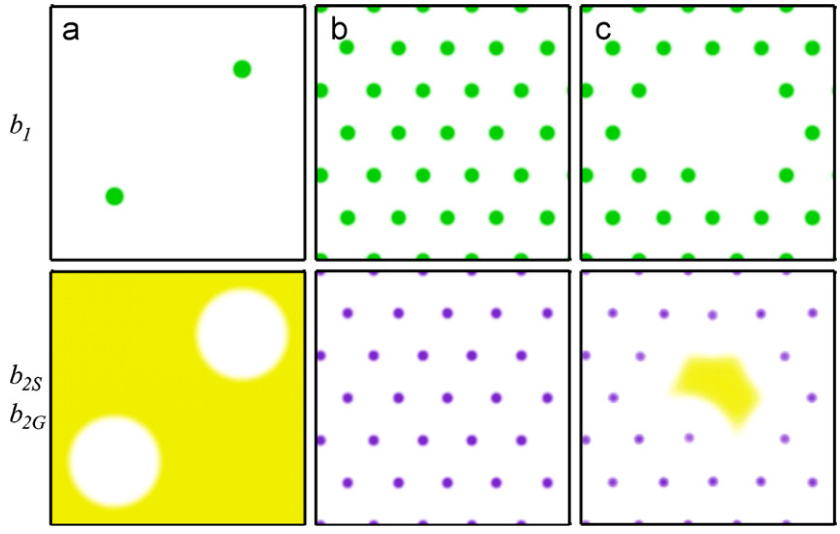

Fig. 11. Effects of woody-patch density on herbaceous-species composition. The green, yellow and purple shades represent, respectively, the spatial biomass distributions of the woody species, b_1, the shading-sensitive herbaceous species, b_{2S}, and the grazing-sensitive herbaceous species, b_{2G}. When the woody patches are sparse (a) the woody species competes and excludes the herbaceous species. In the open space away from the woody patches the grazing-sensitive species cannot cope with the high grazing stress and the shading-sensitive species prevails. When the b_1 patches are dense (b) the woody species facilitates the growth of the herbaceous species under its canopies. In this case the shading-sensitive species cannot survive and the grazing-sensitive species prevails. When the pattern involves regions of sparse and dense patches (c), the two herbaceous species coexist, each in its own niche. The precipitation is $p = 0.55$ (82.5 mm/yr) and all other parameters are as Fig. 7.

The explicit modeling of the infiltration and uptake feedbacks represents a "first-principle" approach whereby community and landscape properties, such as spatial structures, plant interactions and species composition, *emerge* as solutions of the model equations rather than being preset in formulating the model. For example, positive or negative interspecific interactions are not predetermined by the signs of coupling terms in the model equations, as is the case with the Lotka–Volterra model and with some other models (Sandvik et al., 2002), but rather follow from the relative strength of the water–biomass feedbacks that, in turn, is affected by a variety of basic, measurable parameters describing species traits and environmental conditions.

Our study of plant interactions in a mixed woody–herbaceous ecosystem suggests new mechanisms of plant-interaction change in water stressed environments. The mechanisms involve changes in the balance between the infiltration feedback and the uptake feedback (Fig. 5). These changes may result in increased interspecific competition or facilitation, or in complete transitions from competition to facilitation and vice versa. Transitions from competition to facilitation can be induced by aridity stresses (Fig. 4), or by intraspecific patch competition over the water resource (Fig. 7). Both factors act to weaken the water uptake (by reducing the woody-patch size) while leaving the infiltration rate almost unaffected, thereby tilting the balance towards facilitation. Transitions back to competition as the aridity stress further increases can result from the capability of a plant species to further extend its root system in response to an aridity stress (Fig. 6). We also demonstrate how both directions of plant-interaction change, competition to facilitation and facilitation to competition, can be realized along the same environmental gradient. These results shed new light on field observations (Pugnaire and Luque, 2001; Maestre et al., 2005) that are apparently in conflict, and provide possible resolution to the conflict.

The two biomass–water feedbacks are processes that act at the level of a single patch but affect pattern formation at the landscape level by inducing spatial instabilities (Cross and Hohenberg, 1993). Conversely, processes at the landscape level, such as transitions from one pattern state to another, can feed back to the level of a single patch by changing the local soil-water distribution, thereby affecting interspecific interactions. An example of such a cross-scale process (Levin, 1992, 2000) is shown in Fig. 9, where a pattern shift from banded to spotted vegetation on a slope results in the facilitation of herbaceous-species growth in woody patches.

These mechanisms of plant-interaction change bear on species composition as discussed in Section 5 and as Figs. 9–11 demonstrate. Noteworthy is the result that irregular vegetation patterns, involving regions of sparse and dense patches, can support higher species diversity than regular patterns.

Acknowledgments

We thank A. Novoplansky, J. von Hardenberg, A. Provenzale, E. Shefer, A. Kletter and Y. Seligmann for helpful discussions. This study has been supported by the James S. McDonnell Foundation and by the Center for Complexity Science.

Appendix A. Linear stability analysis of stationary homogeneous solutions

A.1. Analysis of the general n-species model

We present here a linear stability analysis of homogeneous stationary solutions of the model equations (7)–(10) for the case of plane topography. Denoting the homogeneous stationary solutions by $\mathbf{U}_0 = (b_{10}, \ldots, b_{n0}, w_0, h_0)^{\mathrm{T}}$, the perturbed solutions are written as

$$\begin{aligned} &\mathbf{U}(\mathbf{x}, t) = \mathbf{U}_0 + \delta\mathbf{U}(\mathbf{x}, t), \\ &\delta\mathbf{U}(\mathbf{x}, t) = \mathbf{a}(t)e^{i\mathbf{k}\cdot\mathbf{x}} + \text{c.c.}, \end{aligned} \tag{A.1}$$

where

$$\begin{aligned} &\mathbf{U} = (b_1, \ldots, b_n, w, h)^{\mathrm{T}}, \\ &\delta\mathbf{U} = (\delta b_1, \ldots, \delta b_n, \delta w, \delta h)^{\mathrm{T}}, \\ &\mathbf{a}(t) = [a_{b_1}(t), \ldots, a_{b_n}(t), a_w(t), a_h(t)]^{\mathrm{T}}, \end{aligned} \tag{A.2}$$

and "c.c." stands for the complex conjugate.

Substitution of the perturbed solution (A.1) into the model equations (7)–(10) gives

$$
\begin{aligned}
(\delta b_i)_t &= G_b^i|_{\mathbf{U}_0+\delta\mathbf{U}}(b_{i0}+\delta b_i)[1-(b_{i0}+\delta b_i)] - \mu_i(b_{i0}+\delta b_i) + \delta_{b_i}\nabla^2(b_{i0}+\delta b_i),\\
(\delta w)_t &= \mathcal{I}|_{\mathbf{U}_0+\delta\mathbf{U}}(h_0+\delta h) - v\left[1-\sum_{i=1}^{n}\rho_i(b_{i0}+\delta b_i)\right](w_0+\delta w) - (w_0+\delta w)\\
&\quad\times\sum_{i=1}^{n} G_w^i|_{\mathbf{U}_0+\delta\mathbf{U}} + \delta_w\nabla^2(w_0+\delta w),\\
(\delta h)_t &= p - \mathcal{I}|_{\mathbf{U}_0+\delta\mathbf{U}}(h_0+\delta h) + \delta_h\nabla^2[(h_0+\delta h)^2],
\end{aligned}
\tag{A.3}
$$

where $i=1,\ldots,n$. Expanding the infiltration term (8) up to first order in δb_i we obtain

$$
\mathcal{I}|_{\mathbf{U}_0+\delta\mathbf{U}} = \mathcal{I}_0 + \sum_{i=1}^{n}\left.\frac{\partial\mathcal{I}}{\partial b_i}\right|_{b_i=b_{i0}}\delta b_i = \alpha\frac{\sum_i\psi_i b_{i0}+qf}{\sum_i\psi_i b_{i0}+q} + \alpha\sum_{i=1}^{n}\frac{\psi_i q(1-f)}{(\sum_k\psi_k b_{k0}+q)^2}\delta b_i + \mathcal{O}(\delta b_i^2). \tag{A.4}
$$

To evaluate the terms $G_b^i|_{\mathbf{U}_0+\delta\mathbf{U}}$ and $G_w^i|_{\mathbf{U}_0+\delta\mathbf{U}}$ we first expand the kernels, $g_i(\mathbf{x},\mathbf{x}')$ and $g_i(\mathbf{x}',\mathbf{x})$ up to first order in δb_i:

$$
\begin{aligned}
g_i(\mathbf{x},\mathbf{x}') &= g_i^0(\mathbf{x},\mathbf{x}') + g_i^1(\mathbf{x},\mathbf{x}')\delta b_i(\mathbf{x}) + \mathcal{O}(\delta b_i^2),\\
g_i(\mathbf{x}',\mathbf{x}) &= g_i^0(\mathbf{x}',\mathbf{x}) + g_i^1(\mathbf{x}',\mathbf{x})\delta b_i(\mathbf{x}') + \mathcal{O}(\delta b_i^2),
\end{aligned}
\tag{A.5}
$$

where

$$
g_i^0(\mathbf{x},\mathbf{x}') = g_i^0(\mathbf{x}',\mathbf{x}) = g_i(\mathbf{x},\mathbf{x}')|_{b_i=b_{i0}} = \frac{1}{2\pi\sigma_i^2}e^{-|\mathbf{x}-\mathbf{x}'|^2/2\xi_i^2},
$$

$$
g_i^1(\mathbf{x},\mathbf{x}') = g_i^1(\mathbf{x}',\mathbf{x}) = \left.\frac{\partial}{\partial b_i}[g_i(\mathbf{x},\mathbf{x}')]\right|_{b_i=b_{i0}} = \frac{\eta_i}{2\pi\sigma_i\xi_i^3}|\mathbf{x}-\mathbf{x}'|^2 e^{-|\mathbf{x}-\mathbf{x}'|^2/2\xi_i^2}. \tag{A.6}
$$

Here, $\xi_i \equiv \sigma_i(1+\eta_i b_{i0})$ and $|\mathbf{x}-\mathbf{x}'|^2 = (x-x')^2+(y-y')^2$.

Substitution of these forms and the perturbed solution in Eqs. (9) and (10), gives

$$
\begin{aligned}
G_b^i|_{\mathbf{U}_0+\delta\mathbf{U}} &= v\lambda_i\int g_i(\mathbf{x},\mathbf{x}')w(\mathbf{x}')\,d\mathbf{x}' \approx v\lambda_i\int[g_i^0(\mathbf{x},\mathbf{x}')+g_i^1(\mathbf{x},\mathbf{x}')\delta b_i(\mathbf{x})][w_0+\delta w(\mathbf{x}')]\,d\mathbf{x}'\\
&= v\lambda_i w_0\int g_i^0(\mathbf{x},\mathbf{x}')\,d\mathbf{x}' + v\lambda_i\int g_i^0(\mathbf{x},\mathbf{x}')\delta w(\mathbf{x}')\,d\mathbf{x}' + v\lambda_i w_0\delta b_i(\mathbf{x})\int g_i^1(\mathbf{x},\mathbf{x}')\,d\mathbf{x}',\\
G_w^i|_{\mathbf{U}_0+\delta\mathbf{U}} &= \gamma_i\int g_i(\mathbf{x}',\mathbf{x})b_i(\mathbf{x}')\,d\mathbf{x}' \approx \gamma_i\int[g_i^0(\mathbf{x}',\mathbf{x})+g_i^1(\mathbf{x}',\mathbf{x})\delta b_i(\mathbf{x}')][b_{i0}+\delta b_i(\mathbf{x}')]\,d\mathbf{x}'\\
&= \gamma_i b_{i0}\int g_i^0(\mathbf{x}',\mathbf{x})\,d\mathbf{x}' + \gamma_i\int g_i^0(\mathbf{x}',\mathbf{x})\delta b_i(\mathbf{x}')\,d\mathbf{x}' + \gamma_i b_{i0}\int g_i^1(\mathbf{x}',\mathbf{x})\delta b_i(\mathbf{x}')\,d\mathbf{x}',
\end{aligned}
\tag{A.7}
$$

where the integration is over the entire domain. Finally, by solving the integrals in Eq. (A.7) we obtain to linear order in the perturbation $\delta\mathbf{U}$:

$$
\begin{aligned}
G_b^i|_{\mathbf{U}_0+\delta\mathbf{U}} &= v\lambda_i w_0(\xi_i/\sigma_i)^2 + v\lambda_i(\xi_i/\sigma_i)^2 e^{-k^2\xi_i^2/2}\delta w(\mathbf{x}) + 2v\lambda_i\eta_i(\xi_i/\sigma_i)w_0\delta b_i(\mathbf{x}),\\
G_w^i|_{\mathbf{U}_0+\delta\mathbf{U}} &= \gamma_i b_{i0}(\xi_i/\sigma_i)^2 + \gamma_i(\xi_i/\sigma_i)e^{-k^2\xi_i^2/2}[1+\eta_i b_{i0}(3-k^2\xi_i^2)]\delta b_i(\mathbf{x}),
\end{aligned}
\tag{A.8}
$$

where $k=|\mathbf{k}|$ is the wavenumber of the perturbation. Using Eqs. (A.4) and (A.8) in Eq. (A.3) and the fact that the stationary homogeneous solutions $\mathbf{U}_0=(b_{10},\ldots,b_{n0},w_0,h_0)^{\mathrm{T}}$ satisfy

$$
\begin{aligned}
0 &= v\lambda_i b_{i0}(1-b_{i0})(\xi_i/\sigma_i)^2 w_0 - \mu_i b_{i0}, \quad i=1,\ldots,n,\\
0 &= \alpha h_0\frac{\sum_i\psi_i b_{i0}+qf}{\sum_i\psi_i b_{i0}+q} - v\left(1-\sum_{i=1}^{n}\rho_i b_{i0}\right)w_0 - w_0\sum_{i=1}^{n}\gamma_i b_{i0}(\xi_i/\sigma_i)^2,\\
0 &= p - \alpha h_0\frac{\sum_i\psi_i b_{i0}+qf}{\sum_i\psi_i b_{i0}+q},
\end{aligned}
\tag{A.9}
$$

we obtain the following system of linear ordinary differential equations for the perturbation amplitudes $\mathbf{a}(t)$:

$$
\frac{da_{b_i}}{dt} = v\lambda_i w_0(\xi_i/\sigma_i)[1-2b_{i0}+\eta_i b_{i0}(3-4b_{i0})-\mu_i-\delta_{b_i}k^2]a_{b_i} + v\lambda_i b_{i0}(1-b_{i0})(\xi_i/\sigma_i)^2 e^{k^2\xi_i^2/2}a_w, \quad i=1,\ldots,n,
$$

$$\frac{da_w}{dt} = \sum_{i=1}^{n}\left\{\frac{\alpha h_0\psi_i q(1-f)}{(\sum_k \psi_k b_{k0}+q)^2} + vw_0\rho_i - w_0\gamma_i(\xi_i/\sigma_i)e^{k^2\xi_i^2/2}[1+\eta_i b_{i0}(3-k^2\xi_i^2)]\right\}a_{b_i}$$
$$-\left[v\left(1-\sum_{i=1}^{n}\rho_i b_{i0}\right)+\sum_{i=1}^{n}\gamma_i b_{i0}(\xi_i/\sigma_i)^2+\delta_w k^2\right]a_w+\alpha\frac{\sum_i\psi_i b_{i0}+qf}{\sum_i\psi_i b_{i0}+q}a_h,$$

$$\frac{da_h}{dt} = -\sum_{i=1}^{n}\left[\frac{\alpha h_0\psi_i q(1-f)}{(\sum_k\psi_k b_{k0}+q)^2}\right]a_{b_i}+\left[\alpha\frac{\sum_i\psi_i b_{i0}+qf}{\sum_i\psi_i b_{i0}+q}-2h_0\delta_h k^2\right]a_h. \tag{A.10}$$

Assuming exponential growth for the perturbation amplitudes, $\mathbf{a}(t)=\mathbf{a}(0)e^{\theta t}$, we obtain the following eigenvalue problem:

$$\theta\mathbf{a}(t)=\mathcal{J}(k)\mathbf{a}(t), \tag{A.11}$$

where $\mathcal{J}(k)\in\mathbb{R}^{(n+2)\times(n+2)}$ is the Jacobian matrix whose entries are given by the terms of Eq. (A.10), and whose explicit forms for $n=1$ and 2 will be given in the next two sections. By solving this eigenvalue problem we obtain dispersion relations of the form $\theta=\theta(k)$, from which we deduce the stability of the stationary homogeneous solutions.

Expressions for the stationary homogeneous solutions $\mathbf{U}_0=(b_{10},\ldots,b_{n0},w_0,h_0)^{\mathrm{T}}$ can be obtained by solving Eqs. (A.9). The bare-soil solution is obtained by substituting $b_{i0}=0$ $(i=1,\ldots,n)$ in these equations which readily leads to $w=p/v$ and $h=p/\alpha f$. The other stationary homogeneous solutions are obtained as follows. Solving the third equation of (A.9) for h_0 we obtain

$$h_0 = p\left[\alpha\frac{\sum_i\psi_i b_{i0}+qf}{\sum_i\psi_i b_{i0}+q}\right]^{-1}. \tag{A.12}$$

Using this equation in the second equation of (A.9) and solving for w_0 we obtain

$$w_0 = p\left[v\left(1-\sum_{i=1}^{n}\rho_i b_{i0}\right)+\sum_{i=1}^{n}\gamma_i b_{i0}(1+\eta_i b_{i0})^2\right]^{-1}. \tag{A.13}$$

The biomass densities b_{i0} in Eqs. (A.12) and (A.13) are either zero or finite, depending on the solution considered. To find the non-zero biomass densities we substitute Eq. (A.13) in the first equation of (A.9) and obtain

$$p=\frac{\mu_j}{\lambda_j}\left[\frac{1-\sum_i\rho_i b_{i0}+\sum_i(\gamma_i/v)b_{i0}(1+\eta_i b_{i0})^2}{(1-b_{j0})(1+\eta_j b_{j0})^2}\right], \tag{A.14}$$

where we used the equality $\xi_j/\sigma_j=1+\eta_j b_{j0}$, and the index j runs over the coexisting species (i.e. whose biomass densities are non-zero). These are implicit equations that can be solved for the non-zero biomass densities.

A.2. Results for the $n=1$ case

According to Eqs. (A.12), (A.13) and (A.14) the stationary uniform solutions $(b_0,w_0,h_0)^{\mathrm{T}}$ of the model equations (7) for the single species are obtained by solving

$$p=\frac{1-\rho b_0+(\gamma/v)b_0(1+\eta b_0)^2}{(1-b_0)(1+\eta b_0)^2}, \tag{A.15}$$

for b_0, if $b_0\neq 0$, and substituting the value of b_0 in

$$w_0 = p[v(1-\rho b_0)+\gamma b_0(1+\eta b_0)^2]^{-1} \tag{A.16}$$

and

$$h_0 = p\left[\alpha\frac{b_0+qf}{b_0+q}\right]^{-1}. \tag{A.17}$$

In obtaining these equations we set $\lambda_1=\mu_1=\sigma_1=\psi_1=1$ (see Table 1).

The Jacobian entries, deduced from Eq. (A.10), are

$$\begin{aligned}
\mathcal{J}_{11} &= (1+\eta b_0)vw_0[1-2b_0+\eta b_0(3-4b_0)]-1-\delta_b k^2,\\
\mathcal{J}_{12} &= vb_0(1-b_0)(1+\eta b_0)^2 e^{-k^2(1+\eta b_0)^2/2},\\
\mathcal{J}_{13} &= 0,\\
\mathcal{J}_{21} &= \alpha h_0\frac{q(1-f)}{(b_0+q)^2}+\rho vw_0-\gamma w_0(1+\eta b_0)e^{-k^2(1+\eta b_0)^2/2}[1+\eta b_0(3-k^2(1+\eta b_0)^2)],\\
\mathcal{J}_{22} &= -v(1-\rho b_0)-\gamma b_0(1+\eta b_0)^2-\delta_w k^2,\\
\mathcal{J}_{23} &= \alpha\frac{b_0+qf}{b_0+q},\\
\mathcal{J}_{31} &= -\alpha h_0\frac{q(1-f)}{(b_0+q)^2},\\
\mathcal{J}_{32} &= 0,\\
\mathcal{J}_{33} &= -\alpha\frac{b_0+qf}{b_0+q}-2\delta_h h_0 k^2.
\end{aligned} \tag{A.18}$$

The bare-soil solution is given by

$$b_0=0,\quad w_0=p/v,\quad h_0=p/\alpha f. \tag{A.19}$$

To study its linear stability we substitute Eqs. (A.19) in Eqs. (A.18) and obtain the Jacobian matrix for this solution:

$$\mathcal{J}(k)=\begin{pmatrix} p-1-\delta_b k^2 & 0 & 0\\ \dfrac{p(1-f)}{qf}-\dfrac{\gamma p e^{k^2/2}}{v}+\rho p & -v-\delta_w k^2 & \alpha f\\ -\dfrac{p(1-f)}{qf} & 0 & -\alpha f-\dfrac{2p\delta_h}{\alpha f}k^2 \end{pmatrix}. \tag{A.20}$$

The eigenvalues of $\mathcal{J}(k)$ are given by the diagonal terms

$$\begin{aligned}
\theta_1(k) &= p-1-\delta_b k^2,\\
\theta_2(k) &= -v-\delta_w k^2,\\
\theta_3(k) &= -\alpha f-\frac{2p\delta_h}{\alpha f}k^2.
\end{aligned} \tag{A.21}$$

The stability of the bare-soil solution is determined by the sign of the largest eigenvalue; negative (positive) sign implies stability (instability). Obviously, $\theta_2<0$ and $\theta_3<0$ for any k, but θ_1 can cross the zero as p is increased, implying an instability of the bare-soil solution. The instability occurs at $p=p_c=1$ and the first mode to grow has zero wavenumber, $k=k_c=0$, as shown in Fig. 3a. A similar analysis can be done for the uniform vegetation solution. The analytic expressions are too long to be displayed here, but the outcome of such an analysis is shown in Fig. 3b. The solution loses stability as p is decreased below a critical value, p_T, in a finite-wavenumber (or Turing-like) instability where the first mode to grow has a non-zero wavenumber k_c (Cross and Hohenberg, 1993).

A.3. Results for the $n=2$ case

The stationary uniform solutions for the two-species case are obtained by solving Eqs. (A.12), (A.13) and (A.14) as follows. The bare-soil solution remains unchanged: $b_{10}=0$, $b_{20}=0$, $w_0=p/v$ and $h_0=p/\alpha f$. The uniform woody-vegetation solution $\mathcal{V}_1$ ($b_1\neq 0$, $b_2=0$) is obtained by solving

$$p=\frac{1-\rho_1 b_{10}+(\gamma_1/v)b_{10}(1+\eta_1 b_{10})^2}{(1-b_{10})(1+\eta_1 b_{10})^2}, \tag{A.22}$$

for b_{10} and substituting the solution and $b_{20}=0$ in Eqs. (A.12) and (A.13) to obtain h_0 and w_0.

The uniform herbaceous vegetation solution $\mathcal{V}_2$ ($b_1 = 0$, $b_2 \neq 0$) is similarly obtained by solving

$$p = \frac{\mu_2}{\lambda_2}\left[\frac{1-\rho_2 b_{20}+(\gamma_2/v)b_{20}(1+\eta_2 b_{20})^2}{(1-b_{20})(1+\eta_2 b_{20})^2}\right], \tag{A.23}$$

for b_{20} and substituting the solution and $b_{10} = 0$ in Eqs. (A.12) and (A.13) to obtain h_0 and w_0.

The uniform mixed vegetation solution, $\mathcal{M}$ ($b_1 \neq 0$, $b_2 \neq 0$), is obtained by solving the coupled equations

$$p = \frac{1-\sum_i \rho_i b_{i0}+\sum_i(\gamma_i/v)b_{i0}(1+\eta_i b_{i0})^2}{(1-b_{10})(1+\eta_1 b_{10})^2}, \tag{A.24}$$

$$p = \frac{\mu_2}{\lambda_2}\left[\frac{1-\sum_i \rho_i b_{i0}+\sum_i(\gamma_i/v)b_{i0}(1+\eta_i b_{i0})^2}{(1-b_{20})(1+\eta_2 b_{20})^2}\right], \tag{A.25}$$

for b_{10} and b_{20} (the index $\imath$ runs over the two species) and substituting the solutions in Eqs. (A.12) and (A.13) to obtain h_0 and w_0.

The points along the p axis where the $\mathcal{V}_1$ and $\mathcal{V}_2$ solutions bifurcate from the bare-soil solution $\mathcal{B}$ can be easily calculated from Eqs. (A.22) and (A.23). Setting $b_{10} = 0$ in Eq. (A.22) leads to the bifurcation point $p = p_{b_1} = 1$ in Fig. 2. Similarly, setting $b_{20} = 0$ in Eq. (A.23) leads to the bifurcation point $p = p_{b_2} = \mu_2/\lambda_2$. Note that these results coincide with the linear stability results obtained for the bare-soil solution in Section 3.

Eqs. (A.22) and (A.23) can also be used to determine whether the bifurcations at $p = p_{b_1}$ and p_{b_2} are supercritical or subcritical, by evaluating the slopes of the $\mathcal{V}_1$ and $\mathcal{V}_2$ solution branches at zero biomass densities:

$$\left.\frac{dp(b_{i0})}{db_{i0}}\right|_{b_{i0}=0} = \frac{\mu_i}{\lambda_i}\left(1-\rho_i+\frac{\gamma_i}{v}-2\eta_i\right). \tag{A.26}$$

A positive (negative) slope implies a supercritical (subcritical) bifurcation. For the parameters used in this work we find

$$1-\rho_1+\frac{\gamma_1}{v}-2\eta_1<0, \quad 1-\rho_2+\frac{\gamma_2}{v}-2\eta_2>0, \tag{A.27}$$

implying that the bifurcations at $p = p_{b_1}$ and at p_{b_2} are subcritical and supercritical, respectively. The saddle-node bifurcation at $p = p_{SDN}$ along the $\mathcal{V}_1$ branch (see Fig. 2) can be calculated by solving

$$\frac{dp(b_{10})}{db_{10}} = 0 \tag{A.28}$$

for b_{10} and substituting the result in Eq. (A.22) to obtain $p_{SDN} = p(b_{10})$.

The linear stability of a stationary uniform solution, $(b_{10}, b_{20}, w_0, h_0)$, is determined by the eigenvalues of the Jacobian matrix whose entries are

$$\mathcal{J}_{11} = v(1+\eta_1 b_{10})w_0[1-2b_{10}+\eta_1 b_{10}(3-4b_{10})]-1-\delta_{b_1}k^2,$$
$$\mathcal{J}_{12} = 0,$$
$$\mathcal{J}_{13} = vb_{10}(1-b_{10})(1+\eta_1 b_{10})^2 e^{-k^2(1+\eta_1 b_{10})^2/2},$$
$$\mathcal{J}_{14} = 0,$$
$$\mathcal{J}_{21} = 0,$$
$$\mathcal{J}_{22} = v\lambda_2(1+\eta_2 b_{20})w_0[1-2b_{20}+\eta_2 b_{20}(3-4b_{20})]-\mu_2-\delta_{b_2}k^2,$$
$$\mathcal{J}_{23} = v\lambda_2 b_{20}(1-b_{20})(1+\eta_2 b_{20})^2 e^{-k^2[\sigma_2(1+\eta_2 b_{20})]^2/2},$$
$$\mathcal{J}_{24} = 0,$$
$$\mathcal{J}_{31} = \frac{\alpha h_0 q(1-f)}{(b_{10}+\psi_2 b_{20}+q)^2}+v\rho_1 w_0 - w_0\gamma_1(1+\eta_1 b_{10})e^{k^2(1+\eta_1 b_{10})^2/2}[1+\eta_1 b_{10}(3-k^2(1+\eta_1 b_{10})^2)],$$
$$\mathcal{J}_{32} = \frac{\alpha h_0 \psi_2 q(1-f)}{(b_{10}+\psi_2 b_{20}+q)^2}+v\rho_2 w_0 - w_0\gamma_2(1+\eta_2 b_{20})e^{k^2[\sigma_2(1+\eta_2 b_{20})]^2/2}[1+\eta_2 b_{20}(3-k^2[\sigma_2(1+\eta_2 b_{20})]^2)],$$

$$
\begin{aligned}
\mathcal{J}_{33} &= -v(1-\rho_1 b_{10}-\rho_2 b_{20})-\gamma_1 b_{10}(1+\eta_1 b_{10})^2-\gamma_2 b_{20}(1+\eta_2 b_{20})^2-\delta_w k^2,\\
\mathcal{J}_{34} &= \alpha\frac{b_{10}+\psi_2 b_{20}+qf}{b_{10}+\psi_2 b_{20}+q},\\
\mathcal{J}_{41} &= -\frac{\alpha h_0 q(1-f)}{(b_{10}+\psi_2 b_{20}+q)^2},\\
\mathcal{J}_{42} &= -\frac{\alpha h_0\psi_2 q(1-f)}{(b_{10}+\psi_2 b_{20}+q)^2},\\
\mathcal{J}_{43} &= 0,\\
\mathcal{J}_{44} &= -\alpha\frac{b_{10}+\psi_2 b_{20}+qf}{b_{10}+\psi_2 b_{20}+q}-2h_0\delta_h k^2.
\end{aligned}
\tag{A.29}
$$

For the bare-soil solution, $b_{10}=0$, $b_{20}=0$, $w_0=p/v$ and $h=p/\alpha f$, we obtain

$$
\mathcal{J}(k)=\begin{pmatrix}
p-1-\delta_{b_1}k^2 & 0 & 0 & 0\\
0 & \lambda_2 p-\mu_2-\delta_{b_2}k^2 & 0 & 0\\
p\left[\dfrac{(1-f)}{qf}-\dfrac{\gamma_1 e^{k^2/2}}{v}+\rho_1\right] & p\left[\dfrac{\psi_2(1-f)}{qf}-\dfrac{\gamma_2 e^{k^2/2}}{v}+\rho_2\right] & -v-\delta_w k^2 & \alpha f\\
-\dfrac{p(1-f)}{qf} & -\dfrac{p\psi_2(1-f)}{qf} & 0 & -\alpha f-\dfrac{2p\delta_h}{\alpha f}k^2
\end{pmatrix}.
$$

The eigenvalues of $\mathcal{J}(k)$ are simply given by the diagonal elements

$$
\begin{aligned}
\theta_1(k) &= p-1-\delta_{b_1}k^2,\\
\theta_2(k) &= \lambda_2 p-\mu_2-\delta_{b_2}k^2,\\
\theta_3(k) &= -v-\delta_w k^2,\\
\theta_4(k) &= -\alpha f-\frac{2p\delta_h}{\alpha f}k^2.
\end{aligned}
\tag{A.30}
$$

The eigenvalues θ_3 and θ_4 are negative for any k. The eigenvalues θ_1 and θ_2, however, can cross the zero: θ_1 first becomes zero for $k=0$ at $p=1$ whereas θ_2 first becomes zero for $k=0$ at $p=\mu_2/\lambda_2$. Thus, the bare-soil solution becomes unstable to homogeneous perturbations at $p=p_c=\min(1,\mu_2/\lambda_2)$.

References

Bertness, M.D., Callaway, R.M., 1994. Positive interactions in communities. Trends Ecol. Evol. 9, 191–193.

Bertness, M.D., Ewanchuk, P.J., 2002. Latitudinal and climate-driven variation in the strength and nature of biological interactions in New England salt marshes. Oecologia 132, 392–401.

Bertness, M.D., Hacker, S.D., 1994. Physical stress and positive associations among marsh plants. Am. Nat. 144, 363–372.

Bloom, A.J., Chapin III, F.S., Mooney, H.A., 1985. Resource limitation in plants—an economic analogy. Annu. Rev. Ecol. Syst. 16, 363–392.

Brooker, R.W., Callaghan, T.V., 1998. The balance between positive and negative plant interactions and its relationship to environmental gradients: a model. Oikos 81, 196–207.

Bruno, J.F., Stachowicz, J.J., Bertness, M.D., 2003. Inclusion of facilitation into ecological theory. Trends Ecol. Evol. 18, 119–125.

Callaway, R.M., Walker, L.R., 1997. Competition and facilitation: a synthetic approach to interactions in plant communities. Ecology 78, 1958–1965.

Callaway, R.M., Brooker, R.W., Choler, P., Kikvidze, Z., Lortiek, C.J., Michalet, R., Paolini, L., Pugnaire, F.I., Newingham, B., Aschehoug, E.T., Armas, C., Kikodze, D., Cook, B.J., 2002. Positive interactions among alpine plants increase with stress. Nature 417, 844–848.

Campbell, S.E., Seeler, J.S., Glolubic, S., 1989. Desert crust formation and soil stabilization. Arid Soil Res. Rehabil. 3, 217–228.

Casper, B.B., 1996. Demographic consequences of drought in the herbaceous perennial Cryptantha flava: effects of density, associations with shrubs, and plant size. Oecologia 106, 144–152.

Cross, M.C., Hohenberg, P.C., 1993. Pattern formation outside of equilibrium. Rev. Mod. Phys. 65, 851–1112.

Gilad, E., von Hardenberg, J., Provenzale, A., Shachak, M., Meron, E., 2004. Ecosystem engineers: from pattern formation to habitat creation. Phys. Rev. Lett. 93, 0981051.

Gilad, E., von Hardenberg, J., Provenzale, A., Shachak, M., Meron, E., 2007. A mathematical model of plants as ecosystem engineers. J. Theor. Biol. 244, 680–691.

Greenlee, J.T., Callaway, R.M., 1996. Effects of abiotic stress on the relative importance of interference and facilitation. Am. Nat. 148, 386–396.

Grover, J.P., 1997. Resource Competition. Chapman & Hall, London.

Gurney, W.S.C., Lawton, J.H., 1996. The population dynamics of ecosystem engineers. Oikos 76, 273–283.

von Hardenberg, J., Meron, E., Shachak, M., Zarmi, Y., 2001. Diversity of vegetation patterns and desertification. Phys. Rev. Lett. 87, 198101.

Hillel, D., 1998. Environmental Soil Physics. Academic Press, San Diego.

House, J., Archer, S., Breshears, D., Scholes, R.J., 2003. Conundrums in mixed woody–herbaceous plant systems. J. Biogeogr. 30, 1763–1777.

Jones, C.G., Lawton, J.H., Shachak, M., 1994. Organisms as ecosystem engineers. Oikos 69, 373–386.

Jones, C.G., Lawton, J.H., Shachak, M., 1997. Positive and negative effects of organisms as ecosystem engineers. Ecology 78, 1946–1957.

Klausmeier, C.A., 1999. Regular and irregular patterns in semiarid vegetation. Science 284, 1826–1828.

Lefever, R., Lejeune, O., 1997. On the origin of tiger bush. B. Math. Biol. 59, 263–294.

Levin, S.A., 1992. The problem of pattern and scale in ecology. Ecology 73, 1943–1967.

Levin, S.A., 2000. Multiple scales and the maintenance of biodiversity. Ecosystems 3, 498–506.

Maestre, F.T., Cortina, J., 2004a. Do positive interactions increase with abiotic stress? A test from a semiarid steppe. Proc. R. Soc. London B (Suppl.) 271, S331–S333.

Maestre, F.T., Cortina, J., 2004b. Are *Pinus halepensis* afforestations useful as a restoration tool in degraded semiarid Mediterranean areas? Forest Ecol. Manage. 198, 303–317.

Maestre, F.T., Bautista, S., Cortina, J., 2003. Positive, negative and net effects in grass–shrub interactions in Mediterranean semiarid grasslands. Ecology 84, 3186–3197.

Maestre, F.T., Valladares, F., Reynolds, J.F., 2005. Is the change of plant–plant interactions with abiotic stress predictable? A meta-analysis of field results in arid environments. J. Ecol. 93, 748–757.

Murray, J.D., 1993. Mathematical Biology, second corrected ed., Biomathematics, vol. 19. Springer, Berlin, Heidelberg.

Okayasu, T., Aizawa, Y., 2001. Systematic analysis of periodic vegetation patterns. Prog. Theor. Phys. 106, 705–720.

Pennings, S.C., Seling, E.R., Houser, L.T., Bertness, M.D., 2003. Geographic variation in positive and negative interactions among salt marsh plants. Ecology 84, 1527–1538.

Pugnaire, F.I., Luque, M.T., 2001. Changes in plant interactions along a gradient of environmental stress. Oikos 93, 42–49.

Rietkerk, M., Boerlijst, M.C., Van Langevelde, F., HilleRisLambers, R., Van de Koppel, J., Kumar, L., Prins, H.H.T., De Roos, A.M., 2002. Self-organization of vegetation in arid ecosystems. Am. Nat. 160, 524–530.

Rietkerk, M., Dekker, S.C., de Ruiter, P.C., Van de Koppel, J., 2004. Self-organized patchiness and catastrophic shifts in ecosystems. Science 305, 1926–1929.

Sandvik, G., Seip, K.l., Pleym, H., 2002. An anatomy of interactions among species in a seasonal world. Oikos 99, 260–271.

Scheffer, M., Carpenter, S., Foley, J.A., Folke, C., Walkerk, B., 2001. Catastrophic shifts in ecosystems. Nature 413, 591–596.

Shachak, M., Sachs, M., Moshe, I., 1998. Ecosystem management of desertified shrublands in Israel. Ecosystems 1, 475–483.

Shnerb, N.M., Sarah, P., Lavee, H., Solomon, S., 2003. Reactive glass and vegetation patterns. Phys. Rev. Lett. 90, 0381011.

Silvertown, J., 2004. Plant coexistence and the niche. Trends Ecol. Evol. 19, 605–611.

Sommer, U., Worm, B. (Eds.), 2002. Competition and Coexistence. Ecological Studies, vol. 161, Springer, Berlin.

Sternberg, M., Shoshany, M., 2001. Influence of slope aspect on Mediterranean woody formation: comparison of a semiarid and an arid site in Israel. Ecol. Res. 16, 335–345.

Tielbörger, K., Kadmon, R., 2000. Temporal environmental variation tips the balance between facilitation and interference in desert plants. Ecology 81, 1544–1553.

Tilman, D., 1982. Resource Competition and Community Structure. Princeton University Press, Princeton, NJ.

Tilman, D., 1988. Plant Strategies and the Dynamics and Structure of Plant Communities. Princeton University Press, Princeton, NJ.

Valentin, C., d'Herbès, J.M., Poesen, J., 1999. Soil and water components of banded vegetation patterns. Catena 37, 1–24.

West, N.E., 1990. Structure and function in microphytic soil crusts in wildland ecosystems of arid and semi-arid regions. Adv. Ecol. Res. 20, 179–223.

Yair, A., Shachak, M., 1987. Studies in watershed ecology of an arid area. In: Wurtele, M.O., Berkofsky, L. (Eds.), Progress in Desert Research. Rowman and Littlefield Publishers, New York, pp. 146–193.